Characteristics of the polarization part of the optical potential for a weakly bound projectile, ^{9}Be

W. Y. So,[1,2] T. Udagawa,[2] K. S. Kim,[3] S. W. Hong,[4] and B. T. Kim[4]

[1]*Department of Radiological Science, Kangwon National University at Dogye, Samcheok 245-907, Korea*

[2]*Department of Physics, University of Texas, Austin, Texas 78712, USA*

[3]*School of Liberal Arts and Science, Korea Aerospace University, Koyang 412-791, Korea*

[4]*Department of Physics and Department of Energy Science, Sungkyunkwan University, Suwon 440-746, Korea*

(Received 12 June 2009; published 8 April 2010)

Based on the extended optical model with the double folding potential, in which the polarization potential is decomposed into direct reaction (DR) and fusion parts, simultaneous χ^2 analyses are performed of elastic scattering and fusion cross-section data for the ^{9}Be + ^{28}Si, ^{144}Sm, and ^{208}Pb systems at near-Coulomb-barrier energies. The polarization potentials thus determined are found to reveal an interesting target mass number dependence reflecting the experimental observation that the fusion cross section becomes larger than the DR cross section as the target changes from ^{208}Pb to ^{28}Si.

DOI: 10.1103/PhysRevC.81.047604 PACS number(s): 24.10.−i, 25.70.Jj

Recently, we have done simultaneous χ^2 analyses of elastic scattering and fusion cross-section data for ^{6}Li, ^{7}Li + ^{208}Pb [1], and ^{12}C + ^{208}Pb [2] systems at near-Coulomb-barrier energies by using the double folding potential [3] and the extended optical model approach [4] in which the polarization potential is decomposed into direct reaction (DR) and fusion parts. Both ^{6}Li and ^{7}Li projectiles are weakly bound nuclei. Thus, it was expected that the resulting real part of the DR potential that might be related to the couplings with the breakup channels would become repulsive as was observed in the CDCC calculations [5,6]. Indeed we obtained repulsive real DR polarization potentials for both ^{6}Li and ^{7}Li projectiles [1]. We also found that the resultant DR potential for the ^{6}Li projectile is more repulsive than that for ^{7}Li, which is also consistent with the CDCC calculations by Keeley and Rusek [6], explaining the normalization factors used in Ref. [3]. In addition, we showed that both DR and fusion potentials satisfied the dispersion relation [7,8] separately.

The ^{9}Be projectile also exhibits a strong breakup character. Thus, if one tries to analyze the elastic scattering data for the systems involving a ^{9}Be projectile by using the usual one-channel optical model with a double folding potential as the bare potential, one is forced to introduce a normalization factor of $N \approx 0.3 \sim 0.6$ [3] as for ^{6}Li. Data for ^{9}Be projectiles have been accumulated enough for both elastic scattering and fusion at energies near the Coulomb-barrier energy for targets such as ^{28}Si [9,10], ^{144}Sm [11], and ^{208}Pb [12,13], so that we can attempt to carry out extended optical model analyses with the double folding potentials for the ^{9}Be + ^{28}Si, ^{144}Sm, and ^{208}Pb systems, following the method used in our previous analyses of Refs. [1,2].

We thus first generate the so-called semiexperimental DR cross section $\sigma_D^{\text{semi-exp}}$ by using the expression $\sigma_D^{\text{semi-exp}} = \sigma_R^{\text{semi-exp}} - \sigma_F^{\text{exp}}$, where $\sigma_R^{\text{semi-exp}}$ is the total reaction cross section obtained from the preliminary simple optical model χ^2 analyses of the elastic scattering data [9–12], while σ_F^{exp} is the experimental fusion cross section taken from Refs. [9–11,13].

After $\sigma_D^{\text{semi-exp}}$ is obtained, we perform the simultaneous χ^2 analyses on the data sets of $(d\sigma_E^{\text{exp}}/d\Omega, \sigma_D^{\text{semi-exp}}, \sigma_F^{\text{exp}})$ by employing $d\sigma_E^{\text{exp}}/d\Omega$ and σ_F^{exp} taken from Refs. [9–13]. The optical potential $U(r, E)$ we use in the simultaneous analyses has the following form:

$$U(r;E) = V_C(r) - [V_0(r) + U_F(r;E) + U_D(r;E)], \qquad (1)$$

where $V_C(r)$ is the usual Coulomb potential with r_C = 1.25 fm and $V_0(r)$ is the bare nuclear potential, for which use is made of the double folding potential. $U_F(r;E)$ and $U_D(r;E)$ are, respectively, fusion and DR parts of the so-called polarization potential that originates from couplings with the respective reaction channels. Both $U_F(r;E)$ and $U_D(r;E)$ are complex $[U_i(r;E) = V_i(r;E) + iW_i(r;E)$, $i = F$ or $D]$ and their forms are assumed to be of volume-type and surface-derivative-type Woods-Saxon function, respectively, with the fixed geometrical parameters $r_i = R_i/(A_1^{1/3} + A_2^{1/3})$ listed in Table I. As explained in details in Ref. [1], to eliminate unphysical oscillations appearing in the radial wave functions of low partial waves, a short-range imaginary potential of the Woods-Saxon type with $W_I = 40$ MeV, $r_I = 0.8$ fm, and $a_I = 0.30$ fm is added [1,2].

By assuming the geometrical parameters of the real and imaginary potentials to be identical, the strength parameters $V_i(E)$ and $W_i(E)$ $(i = F$ or $D)$ can be related through a dispersion relation [7],

$$V_i(E) = V_i(E_s) + \frac{E - E_s}{\pi} \mathrm{P} \int_0^\infty dE' \frac{W_i(E')}{(E' - E_s)(E' - E)}, \qquad (2)$$

where P stands for the principal value and $V_i(E_s)$ is the value of $V_i(E)$ at a reference energy $E = E_s$.

As in Refs. [1,2], we use for the bare nuclear potential $V_0(r)$ the double folding potential of the form of Eq. (5) in Ref. [3]. For the effective nucleon-nucleon interaction v_{NN} involved, use is made of the sum of the M3Y interaction and the knock-on exchange effect. The functional form of the target nuclear matter distribution, $\rho_1(r)$, for ^{28}Si, ^{144}Sm, and ^{208}Pb is assumed to be $\rho_1(r) = (A/Z)\rho_{\text{ch}}(r)$, where $\rho_{\text{ch}}(r)$ is the proton charge distribution adopted from Ref. [14], while the matter distribution of projectile, $\rho_2(r)$, for ^{9}Be is taken from

TABLE I. The values of the diffuseness a_i and the radius parameters r_i ($i = F, D$) used in the simultaneous χ^2 analyses.

	^{28}Si	^{114}Sm	^{208}Pb
r_F(fm)	1.40	1.40	1.40
a_F(fm)	0.50	0.33	0.27
r_D(fm)	1.50	1.50	1.47
a_D(fm)	0.60	0.51	0.57

Refs. [15,16]. We then use the code DFPOT of Cook [17] for evaluating $V_0(r)$.

In the extended optical model, fusion and DR cross sections, σ_F and σ_D, respectively, are calculated by using the following expression [1,2]:

$$\sigma_i = \frac{2}{\hbar v}\langle\chi^{(+)}|\mathrm{Im}[U_i(r;E)]|\chi^{(+)}\rangle \quad (i = F \text{ or } D), \tag{3}$$

where $\chi^{(+)}$ is the usual distorted wave function that satisfies the Schrödinger equation with the full optical model potential $U(r;E)$ in Eq. (1). σ_F and σ_D are thus calculated within the same framework as $d\sigma_{el}/d\Omega$ is calculated. Such a unified description enables us to evaluate all the different types of cross sections on the same footing.

The simultaneous χ^2 analyses are done in two steps [1,2]; in the first step we let all four strength parameters, $V_F(E)$, $W_F(E)$, $V_D(E)$, and $W_D(E)$ vary. In this step, we have been able to fix fairly well the strength parameters of the DR potential, $V_D(E)$ and $W_D(E)$, in the sense that $V_D(E)$ and $W_D(E)$ are determined as a smooth function of E, as shown in Fig. 1 by the open circles. Note that the real part of the resultant DR potential, $V_D(E)$, is systematically repulsive except for the ^{28}Si target. We can represent the extracted values of $W_D(E)$ plotted in the lower panel of Fig. 1 by the following function of E (two linear segments),

$$W_i(E) = \begin{cases} 0 & \text{for } E \leqslant E_0 \\ \alpha(E - E_0) & \text{for } E_0 < E \leqslant E_1, \\ W_1 & \text{for } E_1 < E \end{cases} \tag{4}$$

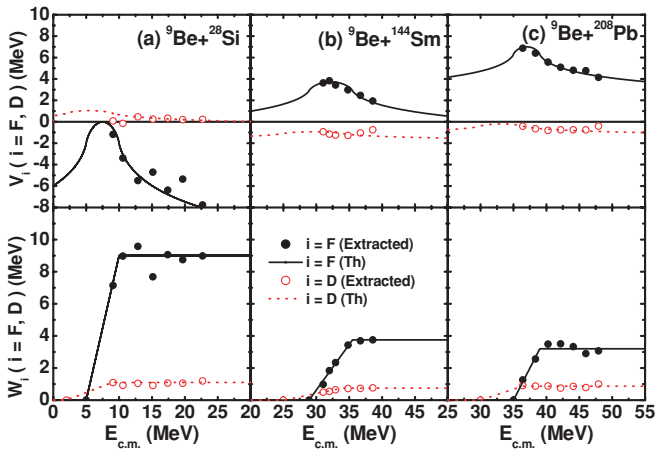

FIG. 1. (Color online) The strength parameters V_i (upper panel) and W_i (lower panel) for $i = D$ (the open circles) and F (the solid circles) as functions of E.

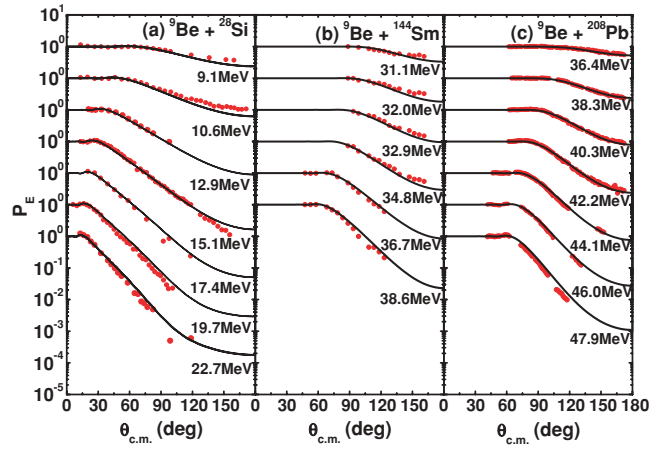

FIG. 2. (Color online) The ratios of the elastic scattering cross sections to the Rutherford cross section calculated with our final dispersive optical potential are shown in comparison with the experimental data. The data are taken from Refs. [9–12] for the ^{28}Si, ^{144}Sm, and ^{208}Pb targets, respectively.

where $i = D$ and the sets of values for (α, W_1, E_0, E_1) are, respectively, (0.157, 1.10, 2.0, 9.0) for ^{28}Si, (0.083, 0.745, 25.0, 34.0) for ^{144}Sm, and (0.136, 0.87, 30.0, 36.4) for ^{208}Pb. (The values of W_1, E_0, E_1, and E are all in units of MeV.) Note that the threshold energies E_0 at which $W_{i=D}(E)$ becomes zero are determined as in [1,2] by using the Stelson plot [18] of $\sigma_D^{\text{semi}-\text{exp}}$.

The dotted lines in the lower panel of Fig. 1 represent the linear seguments expressed by Eq. (4). The dotted lines in the upper panel of Fig. 1 denote $V_D(E)$ as calculated by the dispersion relation of Eq. (2) with $W_D(E)$ given by Eq. (4). As seen, the dotted lines in the upper panel fit the open circles quite well, indicating that $V_D(E)$ and $W_D(E)$ extracted by the χ^2 analyses satisfy the dispersion relation. In this first step of χ^2 fitting, however, the values of $V_F(E)$ and $W_F(E)$ are not reliably fixed in the sense that the extracted values fluctuate considerably as functions of E.

To obtain reliable information on V_F and W_F, we thus have performed the second step of the χ^2 analysis as in Refs. [1,2]. This time, instead of doing a four-parameter search we keep V_D and W_D as determined by the first step of χ^2 fitting, that is, $W_D(E)$ given by Eq. (4) and $V_D(E)$ predicted from the dispersion relation. We then perform two-parameter χ^2 analyses, treating only $V_F(E)$ and $W_F(E)$ as adjustable parameters. The values thus extracted are presented in Fig. 1 by the solid circles. The values of $W_F(E)$ may be represented by the same form of Eq. (4) with $i = F$ and the sets of values of (α, W_1, E_0, E_1) = (1.80, 9.00, 5.0, 10.0), (0.568, 3.75, 28.9, 35.5), and (0.80, 3.20, 35.0, 39.0), respectively, for ^{28}Si, ^{144}Sm, and ^{208}Pb.

As shown in Fig. 1, the $W_F(E)$ values determined by the second step of χ^2 analyses can fairly well be represented by the linear seguments of Eq. (4) with the values of the parameters listed above. Note that the energy variations in both $W_F(E)$ and $V_F(E)$ are more rapid compared to those in $W_D(E)$ and $V_D(E)$, and are similar to those observed with tightly bound

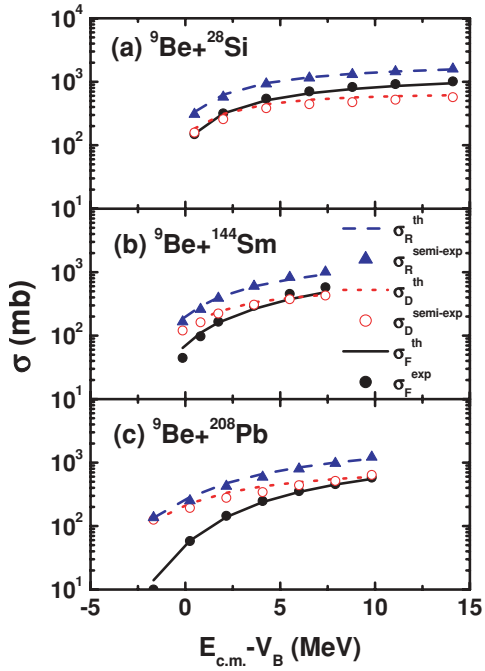

FIG. 3. (Color online) DR and fusion cross sections calculated with our final dispersive optical potentials are shown in comparison with the experimental data. $\sigma_D^{\text{semi}-\text{exp}}$ denoted by the open circles are obtained as described in the text. The Coulomb barrier energies, V_B, are taken as 8.6, 31.2, and 38.1 MeV for the ^{28}Si, ^{144}Sm, and ^{208}Pb targets, respectively, from the Wong's formula [19]. The fusion data are from Refs. [9–11,13].

projectiles [20–22]. It is thus seen that the resultant $V_F(E)$ and $W_F(E)$ exhibit the threshold anomaly.

Using $W_F(E)$ given by the two linear seguments, one can generate $V_F(E)$ from the dispersion relation. The results are shown by the solid curves in the upper panel of Fig. 1, which again well reproduce the values (the solid circles) extracted from the χ^2 fitting. This means that the fusion potential determined from the present analysis satisfies the dispersion relation.

We have performed the final calculations of the elastic, DR, and fusion cross sections, by using $W_D(E)$ and $W_F(E)$ by the linear functions together with $V_D(E)$ and $V_F(E)$ generated from the dispersion relation. The results are presented in Figs. 2 and 3 in comparison with the experimental data. All the data are fairly well reproduced by the calculations. We list in Table II the values of the χ^2 per datum for the scattering cross sections evaluated by assuming 1% errors for all the experimental points.

It is remarkable to find that the polarization potentials determined in the present analyses exhibit interesting target mass number dependence. As seen in Fig. 1, the relative magnitudes of $W_F(E)$ with respect to $W_D(E)$ changes systematically as the target changes from ^{28}Si to ^{208}Pb. As the target mass increases, the ratio of $W_F(E)$ to $W_D(E)$ decreases significantly. Because the geometrical parameters of the fusion and DR potentials differ, the relative importance of these potentials may better be seen by comparing their values at the strong absorption radius $r = R_{\text{sa}}$, that is, $W_F(R_{\text{sa}}; E)$ and $W_D(R_{\text{sa}}; E)$. These

TABLE II. The χ^2 values at all incident energies for ^{9}Be + ^{28}Si, ^{144}Sm, and ^{208}Pb targets.

^{28}Si		^{144}Sm		^{208}Pb	
$E_{c.m.}$	χ^2	$E_{c.m.}$	χ^2	$E_{c.m.}$	χ^2
9.1	8.2	31.1	11.7	36.4	0.2
10.6	18.4	32.0	23.3	38.3	0.1
12.9	3.9	32.9	17.3	40.3	0.4
15.1	8.7	34.8	25.0	42.2	0.9
17.4	93.8	36.7	9.6	44.1	0.9
19.7	45.3	38.6	57.7	46.0	2.0
22.7	47.4			47.9	30.7

values together with the sum $W_{\text{tot}}(R_{\text{sa}}; E) = W_F(R_{\text{sa}}; E) + W_D(R_{\text{sa}}; E)$ are plotted in the left panel of Fig. 4 as functions of E for the three targets considered. It can be seen that at $r = R_{\text{sa}}$ the total imaginary potential is dominated by the DR part for ^{208}Pb, but for ^{28}Si the fusion part becomes larger than the DR part.

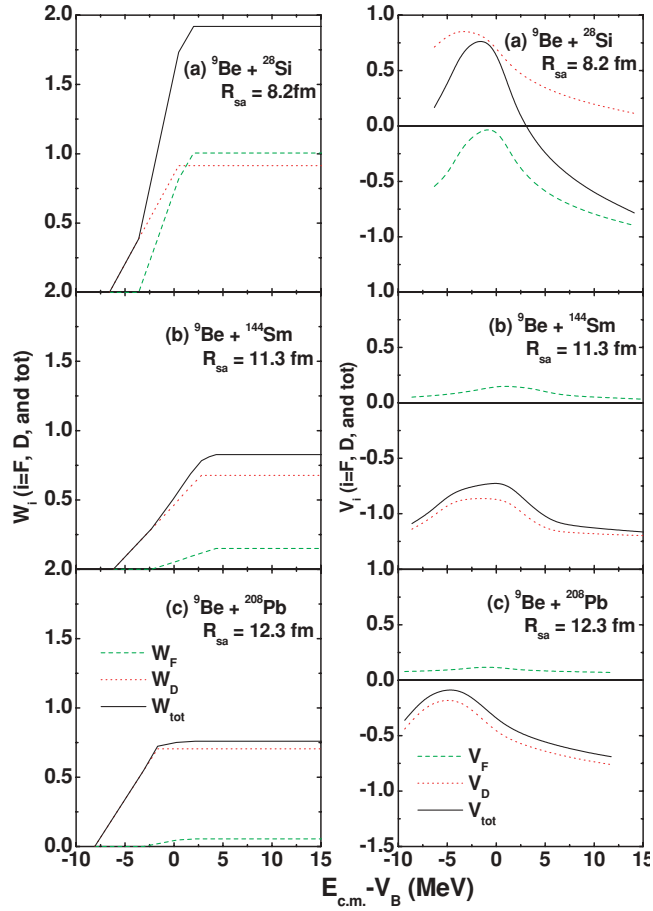

FIG. 4. (Color online) The values of $W_F(R_{\text{sa}}, E)$, $W_D(R_{\text{sa}}, E)$ and the sum $W_{\text{tot}}(R_{\text{sa}}, E) = W_F(R_{\text{sa}}, E) + W_D(R_{\text{sa}}, E)$ at the strong absorption radius are plotted as functions of $E_{\text{c.m.}} - V_B$ for (a) the ^{9}Be + ^{28}Si system, (b) the ^{9}Be + ^{144}Sm system, and (c) the ^{9}Be + ^{208}Pb system. The values of $V_F(R_{\text{sa}}, E)$, $V_D(R_{\text{sa}}, E)$ and the sum $V_{\text{tot}}(R_{\text{sa}}, E)$ are plotted in the right panel.

This change in the relative importance between $W_F(r;E)$ and $W_D(r;E)$ seems to reflect the features of the experimental data plotted in Fig. 3. The ratio of the experimental fusion cross section relative to the semiexperimental DR cross section, $R = \sigma_F^{\rm exp}/\sigma_D^{\rm semi-exp}$ is larger than unity for ^{28}Si, but becomes much smaller than unity for ^{208}Pb. The DR cross section is much larger than the fusion cross section for a heavy target. For a midsized target of ^{144}Sm, the situation is in between ^{28}Si and ^{208}Pb. This enhancement of the DR cross section for heavier targets may be caused by the stronger effects of the Coulomb force.

The target mass number dependence appears also in the values of the real part of the polarization potential, $V_F(E)$ and $V_D(E)$, shown in the right panel of Fig. 4; the values of $V_D(E)$ plotted by the dotted curves are negative (repulsive) for ^{144}Sm and ^{208}Pb but become positive (attractive) for ^{28}Si. The values of $V_F(E)$ denoted by the dashed curves behave in a completely opposite way; they are positive (attractive) for ^{144}Sm and ^{208}Pb, but negative (repulsive) for ^{28}Si. The repulsive nature of $V_D(r;E)$ for ^{144}Sm and ^{209}Pb and $V_F(r;E)$ for ^{28}Si seems to come from the coupling of the elastic channel with the incomplete fusion and fusion channels through those of breakup.

We finally remark on the normalization factor for the double folding potential. The right panel of Fig. 4 shows the total real polarization potential $V_{\rm tot}(R_{\rm sa};E)$ is repulsive for all three targets and energies, except at the lower energies for ^{28}Si. This comes from the repulsiveness of $V_D(E)$ for ^{144}Sm and ^{208}Pb and of V_F for ^{28}Si. Because $V_{\rm tot}(R_{\rm sa},E)$ is repulsive, we can reproduce the elastic scattering data without introducing a normalization factor N to the double folding potential as was necessary in [3]. Similar results were obtained in [6] and in our previous studies [1] showing the need of the repulsive real polarization potential for the ^{6}Li + ^{208}Pb and ^{7}Li + ^{208}Pb systems.

It should be noted, however, that the detailed quantitative nature of the polarization potential may depend on what we use for the double folding potential. In this work, use is made of that obtained from the M3Y interaction, but in recent years effective interactions including the density dependence such as DDM3Y have been developed. It would be an interesting future work to repeat the present analyses and also CDCC calculations by using such an improved interaction to get more quantitative information about the polarization potential.

ACKNOWLEDGMENTS

This work was supported in part by the National Research Foundation grant funded by the Korean government (MEST) (Grant Nos. 2009-0067169 and 2009-0077715) and the WCU program through the National Research Foundation (R31-2008-000-10029-0).

[1] W. Y. So, T. Udagawa, K. S. Kim, S. W. Hong, and B. T. Kim, Phys. Rev. C **75**, 024610 (2007); **76**, 024613 (2007).
[2] W. Y. So, T. Udagawa, S. W. Hong, and B. T. Kim, Phys. Rev. C **77**, 024609 (2008).
[3] G. R. Satchler and W. G. Love, Phys. Rep. **55**, 183 (1979).
[4] T. Udagawa, B. T. Kim, and T. Tamura, Phys. Rev. C **32**, 124 (1985); T. Udagawa and T. Tamura, *ibid.* **29**, 1922 (1984).
[5] Y. Sakuragi, Phys. Rev. C **35**, 2161 (1987).
[6] N. Keeley and K. Rusek, Phys. Lett. B **427**, 1 (1998).
[7] C. Mahaux, H. Ngô, and G. R. Satchler, Nucl. Phys. A **449**, 354 (1986); **456**, 134 (1986).
[8] M. A. Nagarajan, C. C. Mahaux, and G. R. Satchler, Phys. Rev. Lett. **54**, 1136 (1985).
[9] K. Bodek *et al.*, Nucl. Phys. A **339**, 353 (1980).
[10] M. Hugi *et al.*, Nucl. Phys. A **368**, 173 (1981).
[11] P. R. S. Gomes *et al.*, Phys. Rev. C **73**, 064606 (2006).
[12] R. J. Woolliscroft, B. R. Fulton, R. L. Cowin, M. Dasgupta, D. J. Hinde, C. R. Morton, and A. C. Berriman, Phys. Rev. C **69**, 044612 (2004).
[13] M. Dasgupta *et al.*, Phys. Rev. Lett. **82**, 1395 (1999).
[14] C. W. De Jager, H. DeVries, and C. DeVries, At. Data Nucl. Data Tables **14**, 479 (1974).
[15] V. Hnizdo, J. Szymakowski, W. Kemper, and J. D. Fox, Phys. Rev. C **24**, 1495 (1981).
[16] Y. L. Ye *et al.*, Phys. Rev. C **71**, 014604 (2005).
[17] J. Cook, Comput. Phys. Commun. **25**, 125 (1982).
[18] P. H. Stelson, Phys. Lett. B **205**, 190 (1988); P. H. Stelson, H. J. Kim, M. Beckerman, D. Shapira, and R. L. Robinson, Phys. Rev. C **41**, 1584 (1990).
[19] C. Y. Wong, Phys. Rev. Lett. **31**, 766 (1973).
[20] A. Baeza *et al.*, Nucl. Phys. A **419**, 412 (1984).
[21] J. S. Lilley *et al.*, Phys. Lett. B **151**, 181 (1985).
[22] B. R. Fulton *et al.*, Phys. Lett. B **162**, 55 (1985).